

Positional ordering of hard adsorbate particles in tubular nanopores

Péter Gurin,¹ Szabolcs Varga,¹ Yuri Martínez-Ratón,² and Enrique Velasco³

¹*Institute of Physics and Mechatronics, University of Pannonia,
P.O. Box 158, Veszprém H-8201, Hungary*

²*Grupo Interdisciplinar de Sistemas Complejos (GISC), Departamento de Matemáticas,
Escuela Politécnica Superior, Universidad Carlos III de Madrid,
Avenida de la Universidad 30, E-28911, Leganés, Madrid, Spain*

³*Departamento de Física Teórica de la Materia Condensada,
Instituto de Física de la Materia Condensada (IFIMAC)
and Instituto de Ciencia de Materiales Nicolás Cabrera,
Universidad Autónoma de Madrid, E-28049 Madrid, Spain*

(Dated: May 7, 2019)

Abstract

The phase behaviour and structural properties of a monolayer of hard particles is examined in such a confinement, where the adsorbed particles are constrained to the surface of a narrow hard cylindrical pore. The diameter of the pore is chosen such that only first and second neighbour interactions occur between the hard particles. The transfer operator method of Percus and Zhang [Mol. Phys., 69, 347 (1990)] is reformulated to obtain information about the structure of the monolayer. We have found that a true phase transition is not possible in the examined range of pore diameters. The monolayer of hard spheres undergoes a structural change from fluid-like order to a zigzag-like solid one with increasing surface density. The case of hard cylinders is different in the sense that a layering takes place continuously between a low density one-row and a high density two-row monolayer. Our results reveal a clear discrepancy with classical density functional theories, which do not distinguish smectic-like ordering in bulk from that in narrow periodic pores.

I. INTRODUCTION

There is a growing number of experimental and theoretical studies to understand the nature of glassy behaviours, jamming properties and phase transitions of confined nanoparticles [1–14]. This is mainly due to the progress made in the experimental realization of nanoconfined colloidal systems where the confinement reduces the dimensionality of the system in such an extent that almost two- and even one-dimensional systems can be made. This can be done with confining the particles between two parallel plates [15] and with absorption of the particles into tubular nanopores [16–18]. The order of phase transitions often changes, the systems become frustrated and even new structures appear in the confined geometries as a result of competition between particle-particle and particle-wall interactions. In the case of slit-like pore (parallel plates) it is often found that the first order nature of the phase transitions such as the fluid-solid weakens with the decreasing pore width and a Kosterlitz-Thouless type continuous transition emerges in very narrow pores [19, 20]. Similar phenomenon happens in the cylindrical pore, too, with a difference that no signs of the bulk first order transitions can be observed below a critical radius of the pore because the system becomes practically one-dimensional (1d) where the particles are not allowed to pass each other [21–23]. Moreover, new types of orientationally and positionally ordered structures emerge with the positional restriction such as the triatic, tetratic, hexatic and helical arrangements [24–30]. In confined liquid crystals the phase behaviour is even richer due to the additional orientational freedom. However, similar trends can be observed in the phase behaviour of confined spherical particles as the phase transitions between different mesophases can be suppressed with geometrical confinements [31–33].

In the geometrically frustrated systems, Monte Carlo and molecular dynamics simulations can be inefficient and very slow to find the equilibrium structures due to the slowing down of the dynamics and the presence of only few numbers of microstates connecting the competing structures. As a result they often predict metastable phases and overestimate the order of the phase transitions [34–37]. In addition to this, the predictions of mean field and density functional theories can be even worse as they do not properly include the effect of anisotropic and long ranged correlations. To remedy the above problems, exactly solvable models can be the guideline for both simulation and density functional studies. In this regard exact results are available only for lattice-models and for some quasi-one-dimensional (q1d) continuum

models [38–46]. It is also helpful that the true phase transition is forbidden in 1d system if the pair potential is short ranged [47, 48]. In confined hard body models the knowledge of densest or close packing structures can be also useful. For example, the densest structure of hard spheres in cylindrical tube is very rich showing achiral and chiral configurations with changing the diameter of the cylinder [27, 29].

In this study we examine the phase behaviour of hard bodies, which are adsorbed on the inner surface of the hard cylindrical pore. We resort to the transfer operator method (TOM), which proved to be very successful for several q1d systems such as the system of hard disks between two lines and that of hard spheres in cylindrical pores [49–53] and the system of freely rotating hard objects constrained to a straight line [54–56]. It is also applied with less success in narrow periodic box to mimic the phase behaviour of the bulk two-dimensional systems [49]. In these studies the transfer operator is constructed in such a way that the positional freedom along the channel is integrated out completely and the transverse or the orientational freedom of particles kept in the integral operator. This method serves the exact Gibbs free energy and the transverse positional or the orientational distributions of the particles for systems with only first neighbour interactions. The extension of the method has been done recently for wider pores, where first and second neighbour interactions are present [57, 58]. The fluid of hard squares confined inside a two-dimensional infinite channel defined by two hard walls was also studied within the TOM and density functional theory [59]. The results from both theories compared very well. However the behaviour of this system is completely different from that of the present system, due to the different transverse boundary condition used. In the work of Percus and Zhang [60], the relative coordinates are used to construct the transfer operator of hard squares in periodic box with first and second neighbor interactions between particles. Their method was used to obtain the equation of state of hard squares to see the deviation from the strictly 1d system of hard rods and to see the similarity with the two-dimensional system of parallel hard squares. They found that there is no thermodynamic singularity, i.e. true phase transition cannot occur in their system.

We follow the route of [60] with a modification of the transfer operator which serves both the exact thermodynamics and the distribution function of the first neighbors, too. With the new TOM we show that hard spheres form a zigzag structure while hard cylinders align into two rows with increasing pressure. It is important to emphasize that the structural transi-

tions from a low density fluid phase to these high density structures are smooth without any thermodynamic singularity. Our results are in contrast with some recent density functional and Monte Carlo studies related to similar systems. In Ref. [61] a nematic–smectic phase transition was found for oriented hard rectangles adsorbed on a cylinder, and in Ref. [62] isotropic–nematic and nematic–smectic phase transitions were found for freely rotating hard rectangles on a cylindrical surface. In Ref. [35] the authors find an anomalous structural transition of freely rotating hard squares confined into a narrow channel which has quite similar behaviour as a first order phase transition. Note that such a behavior is not observed in the present models. Furthermore, in contrast to the freely rotating hard squares, see Ref. [63], there is no critical behaviour in the infinite pressure limit. Finally, in the present study we also shed light on the failure of density functional theories, when they are applied to systems in narrow periodic pores.

II. THE CYLINDRICAL PORE AND THE ADSORBED HARD PARTICLES

We assume that the adsorbent has cylindrical shape, it is infinitely long and its inner surface is smooth. Two types of hard particles are inserted into the pore; 1) the hard spheres with diameter σ and 2) the hard cylinders with length L and diameter σ . It is also assumed that the cylinders are orientated along the direction of the pore as the pore is very narrow. Furthermore, the adsorbate particles are always in contact with surface of the pore, but they are allowed to move freely on the surface of the adsorbent. This means that the system has only axial and circular freedom, while the positional freedom is switched off in the radial direction. The diameter of the pore is $W = D + \sigma$, where D is a diameter of a cylinder on which the center of the adsorbate particles can move. We study the phase behaviour of hard spheres and that of hard cylinders in very narrow pores, where only first and second neighbour interactions are possible. In Fig. 1 we show the cartoons of the confined cylinders. Here it is also shown that the system of confined hard cylinder corresponds to a system of hard rectangles moving in a narrow stripe with the periodic boundary condition, where the side lengths of the rectangles are L and $\sigma_e = D \arcsin(\sigma/D)$ along the axial and circular directions, respectively. The latter one, σ_e is a contact distance between two cylinders along the circular direction. Note that the system of confined hard spheres cannot be mapped easily into a stripe where the interacting two-dimensional objects are moving, because the

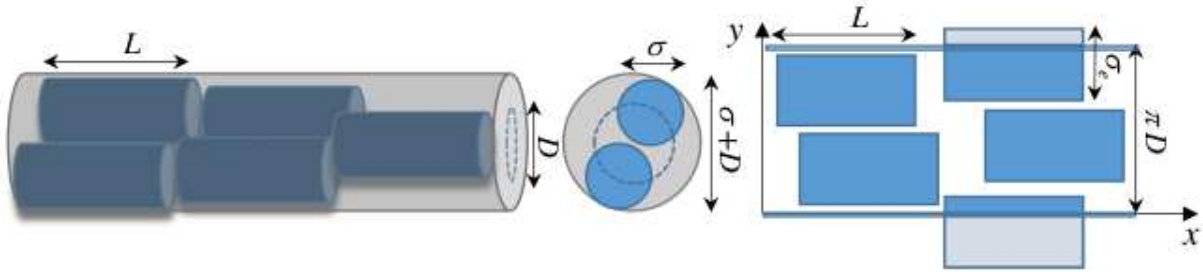


FIG. 1. Schematic of the hard cylinders with diameter σ and length L , which are confined to the inner surface of a cylindrical pore. The centers of the particles are allowed to move on the surface of a cylinder with diameter D , which is shown as dashed circle. The unrolled cylindrical surface having side lengths L_x and $L_y = \pi D$ along x and y directions, respectively, and the projection of hard cylinder particles corresponding hard rectangles are shown in the right panel. The examined system corresponds to system of hard rectangles with side lengths L and σ_e , where the particles are moving in a periodic narrow box.

In the following sections we derive the Gibbs free energy, the equation of state and the nearest neighbour distribution function in the unrolled coordinate frame of the cylindrical surface, where the x axis is along the axial direction, while the y one corresponds to the circular one. We use the notation L_x and L_y for the axial and circular dimension of the surface.

III. THE TRANSFER OPERATOR METHOD

The circular length of our system, L_y , is fixed. However, it turns out that instead of an isochoric ensemble it is more convenient to examine the phase behavior in a mixed isobaric-isochoric ensemble, where the independent variables are the number of particles inside the pore, N , axial force, F_x , and L_y . As the particle-particle and the particle-surface interactions are hard repulsive, the temperature (T) does not play a role in the phase behavior of the system. Consequently, the configuration part of the corresponding partition function

depends on N , $f_x = \beta F_x$ and L_y as follows

$$Z_N(f_x, L_y) = \frac{1}{N!} \int_0^\infty dL_x e^{-f_x L_x} \int_0^{L_y} \left(\prod_{i=1}^N d\hat{y}_i \right) \int_0^{L_x} \left(\prod_{i=1}^N d\hat{x}_i \right) e^{-\beta \sum_{i<j} V(\hat{x}_i, \hat{y}_i, \hat{x}_j, \hat{y}_j)}, \quad (1)$$

where $\beta = 1/k_B T$, the coordinates of the i -th particle are (\hat{x}_i, \hat{y}_i) and the total interaction energy of the system is the sum of the pair potentials, V . Restricting the domain of the integration in Eq.(1) for a fixed order of the particles, $\hat{x}_1 \leq \dots \leq \hat{x}_N$, we can omit the prefactor $1/N!$ because the interparticle potential is symmetric under the permutation of particles. Due to the fact that our system is q1d and the interaction is short ranged, i.e. the potential energy depends only on the relative coordinates of the near neighbours, the integrals of Eq.(1) can be expressed as a product of transfer operators. To obtain that form, as a first step, we change the integration variables to relative coordinates as follows: $(\hat{x}_1, \dots, \hat{x}_N, L_x) \rightarrow (x_0, \dots, x_N)$ and $(\hat{y}_1, \dots, \hat{y}_N) \rightarrow (y_0, \dots, y_{N-1})$ where $x_0 = \hat{x}_1$, $x_i = \hat{x}_{i+1} - \hat{x}_i$, $x_N = L_x - \hat{x}_N$ and $y_0 = \hat{y}_1$, $y_i = (\hat{y}_{i+1} - \hat{y}_i) \bmod L_y$, ($i = 1, \dots, N-1$). With these new variables the configurational integral can be written as

$$Z_N(f_x, L_y) = \int_0^{L_y} \left(\prod_{i=0}^{N-1} dy_i \right) \int_0^\infty \left(\prod_{i=0}^N dx_i \right) e^{-\beta (\sum_{i=1}^{N-1} V(x_i, y_i) + \sum_{i=1}^{N-2} V(x_i + x_{i+1}, y_i + y_{i+1})) - f_x \sum_{i=0}^N x_i}. \quad (2)$$

Here we supposed that only nearest and next nearest neighbour interactions are present which gives an upper limit for L_y . Here and in the followings we mean that the particles are nearest neighbours in the distance x only and not in the real distance, $r = \sqrt{x^2 + y^2}$. Now we rewrite the exponential term of the integrand with a special grouping, with left and right boundary terms being separated from the bulk one, which is symmetric in its variables. This procedure results in

$$e^{-\frac{\beta}{2} V(x_1, y_1) - f_x (x_0 + \frac{x_1}{2})} e^{-\sum_{i=1}^{N-2} \left[\beta \left(\frac{1}{2} V(x_i, y_i) + V(x_i + x_{i+1}, y_i + y_{i+1}) + \frac{1}{2} V(x_{i+1}, y_{i+1}) \right) + f_x \frac{x_i + x_{i+1}}{2} \right]} \times e^{-\frac{\beta}{2} V(x_{N-1}, y_{N-1}) - f_x \left(\frac{x_{N-1}}{2} + x_N \right)}. \quad (3)$$

Using this expression we can write the partition function as an operator product of the middle symmetric terms, while the first and the last terms, together with the integrals of their variables, act as a linear operator on the operator product as follows

$$Z_N(f_x, L_y) = \varphi(\hat{K}^{N-2}). \quad (4)$$

Here \hat{K} is the transfer integral operator which is defined by the kernel

$$K(x, y; x', y') = e^{-\beta(\frac{1}{2}V(x,y)+V(x+x',y+y')+\frac{1}{2}V(x',y'))-f_x\frac{x+x'}{2}}, \quad (5)$$

and $\varphi(\hat{T})$ is a linear functional,

$$\begin{aligned} \varphi(\hat{T}) = & \int_0^{L_y} dy_0 dy_1 dy_{N-1} \int_0^\infty dx_0 dx_1 dx_{N-1} dx_N \\ & e^{-\frac{\beta}{2}V(x_1,y_1)-f_x(x_0+\frac{x_1}{2})} T(x_1, y_1; x_{N-1}, y_{N-1}) e^{-\frac{\beta}{2}V(x_{N-1},y_{N-1})-f_x(\frac{x_{N-1}}{2}+x_N)}. \end{aligned} \quad (6)$$

Note that the partition function of several q1d systems can be written in the form of Eq.(4) where the exponent of the transfer operator and the linear functional φ depends on the specific boundary conditions. However, the concrete form of φ is not important, because the boundary effects do not change the thermodynamic properties of the system.

According to the most general form of the Perron–Frobenius–Jentzsch theorem, see [48], in the thermodynamic limit the Gibbs free energy density is given by $\beta g = -\lim_{N \rightarrow \infty} \frac{1}{N} \ln Z_N = -\ln \lambda_0$, where λ_0 is the (unique) largest solution of the following eigenvalue equation

$$\lambda_k \psi_k(x, y) = \int_0^\infty dx' \int_0^{L_y} dy' K(x, y; x', y') \psi_k(x', y'). \quad (7)$$

In our case the kernel of the transfer operator is defined by Eq. (5). The equation of state can be obtained from the standard thermodynamic relation between the Gibbs free energy and the force, which is now $\rho^{-1} = \partial(\beta g)/\partial f_x$, where $\rho = N/L_x$ is the linear density. Moreover, the expectation value of any quantity $A(x, y)$, which depends only on the relative positions (x and y) of nearest neighbour particles can be expressed by ψ_0 as

$$\langle A \rangle = \int_0^\infty dx \int_0^{L_y} dy A(x, y) |\psi_0(x, y)|^2. \quad (8)$$

As a special case of Eq (8), the distribution function, $f(x, y)$, which describes the probability of finding a *nearest neighbour* pair in relative position x and y is given simply by

$$f(x, y) = |\psi_0(x, y)|^2. \quad (9)$$

Furthermore, we define two nearest neighbour distribution functions for x and y distances as

$$f(x) = \int_0^{L_y} dy f(x, y), \quad (10)$$

and

$$f(y) = \int_0^\infty dx f(x, y). \quad (11)$$

The spatial correlation function of a quantity A can be also expressed by the eigenfunctions and eigenvalues,

$$\begin{aligned} G_A(n) &:= \langle A(x_0, y_0)A(x_n, y_n) \rangle - \langle A(x_0, y_0) \rangle \langle A(x_n, y_n) \rangle \\ &= \sum_{k \geq 1} \left(\frac{\lambda_k}{\lambda_0} \right)^n \left| \int_0^\infty dx \int_0^{L_y} dy \psi_0(x, y) A(x, y) \psi_k(x, y) \right|^2, \end{aligned} \quad (12)$$

where n plays the role of a dimensionless discrete measure of the distance between the 0th and n^{th} nearest neighbour pairs (the real distance is n/ρ on average). The absolute value in Eq. (12) is necessary, however in Eq. (8) and (9) it is only formal, because in general case ψ_k can be complex function, however ψ_0 is always real and positive. A dimensionless correlation length, ξ , is defined by the large distance asymptotic behaviour of the correlation function via the formula $G_A(n) \sim e^{-n/\xi}$, therefore it follows from Eq. (12) that $\xi^{-1} = -\ln(\lambda_1/\lambda_0)$, because the leading term of the sum in Eq. (12) corresponds to $k = 1$ and all the others become negligible as $n \rightarrow \infty$.

We must mention here that the definition of the transfer operator is not unique. If we use the following rearrangement of the integrand of Eq.(2) , instead of Eq.(3),

$$e^{-f_x x_0} e^{-\sum_{i=1}^{N-2} [\beta(V(x_i, y_i) + V(x_i + x_{i+1}, y_i + y_{i+1})) + f_x x_i]} e^{-\beta V(x_{N-1}, y_{N-1}) - f_x (x_{N-1} + x_N)}, \quad (13)$$

we obtain the transfer operator of Percus and Zhang, see Eq. (3.7) in ref. [60], but in this case the computation of the distribution functions is more complicated, since both the left and the right hand side eigenfunctions should be needed. The benefit of the form of Eq. (5) is that the kernel of the transfer operator is symmetric and therefore the left and right eigenfunctions are the same. As a results it is easy to compute the distribution function of the nearest neighbor particles.

A. Hard spheres on a cylindrical surface: the nearest neighbour case

As a first example we apply the above described formalism for hard spheres confined into a narrow cylindrical pore. The diameter of the spheres is denoted by σ , they are absorbed

on the inner surface of a pore with diameter $D + \sigma$, therefore the centers of the spheres can move on a cylinder with diameter D . In this geometry, the explicit form of the hard body interaction gives

$$e^{-\beta V(x,y)} = \theta(x^2 + D^2 \sin^2(y/D) - \sigma^2), \quad (14)$$

where θ is the Heaviside step function. We note that in Eq. (5) the prefactor $1/2$ before the nearest neighbour potential energy is unimportant in the case of hard body interaction, but it is necessary in other cases. We emphasize here a substantial difference between the system of hard spheres on a cylindrical surface and the system of hard disks in a flat 2d channel with periodic boundary conditions. The x projection of the contact distance around its minimum value depends linearly on $|y - y_{\min}|$ in the case of disks but it is quadratic in the case of spheres. Therefore the high axial force limiting behaviours of these systems are different. We discuss this point in the Conclusion.

When $D < \frac{\sqrt{3}}{2}\sigma$, only nearest neighbour interactions take place and the next nearest neighbour term is missing from the exponents of Eq. (5), therefore the kernel can be written as a product of x, y and x', y' dependent factors,

$$K(x, y; x', y') = \theta(x^2 + D^2 \sin^2(y/D) - \sigma^2) e^{-f_x \frac{x}{2}} \theta(x'^2 + D^2 \sin^2(y'/D) - \sigma^2) e^{-f_x \frac{x'}{2}}. \quad (15)$$

In this case the solution of the eigenvalue equation is straightforward and we find that the only eigenfunction which corresponds to a nonzero eigenvalue has the following form

$$\psi_0(x, y) = A \theta(x^2 + D^2 \sin^2(y/D) - \sigma^2) e^{-f_x \frac{x-\sigma}{2}} \quad (16)$$

where A is a normalization constant. All the other functions which are orthogonal to ψ_0 correspond to zero eigenvalue. The largest eigenvalue is given by

$$\begin{aligned} \lambda_0 &= \int_0^{D\pi} dy \int_0^\infty dx \theta(x^2 + D^2 \sin^2(y/D) - \sigma^2) e^{-f_x x} \\ &= \frac{1}{f_x} \int_0^{D\pi} dy e^{-f_x \sqrt{\sigma^2 - D^2 \sin^2(y/D)}} \end{aligned} \quad (17)$$

The fact that all the other eigenvalues are zero reflects the q1d nature of the system. From Eq.(12) we can see that the correlation function of any quantity which depends only on the relative positions of the nearest neighbour particles is identically zero, showing that there are no any correlation between the relative positions, i.e. they are statistically independent variables. As a consequence, the two-particle distribution function can be written

as a convolution of the nearest-neighbour distribution function $f(x, y)$, similar to the case of strictly 1d system of hard rods [64].

B. Parallel cylinders on a cylindrical surface: the next-nearest neighbour case

Here we solve the eigenvalue equation for cylinders with diameter σ and length L absorbed at the inner surface of a pore which diameter is $D + \sigma$. All the cylinders are parallel with the pore. Again, as in case of the spheres, the centers of the particles can move on a cylinder with diameter D and $L_y = D\pi$. Now, due to the hard body interactions, we can write

$$e^{-\beta V(x,y)} = 1 - \theta(L - x) \theta(\sigma - D |\sin(y/D)|) \quad (18)$$

When $D < \sigma$, only nearest neighbour interactions take place, and the system forms a simple 1d Tonks gas. When $\sigma < D < \frac{2}{\sqrt{3}}\sigma$, next-nearest neighbour interactions take place, too, but not third neighbour interactions, therefore our formalism can be applied. Using Eqs. (18) and (5), it is worth writing down Eq. (7) into two regions of x . For $x > L$ (it follows that $\theta(L - x) = \theta(L - (x + x')) = 0$) we have

$$\begin{aligned} \lambda_k \psi_k(x, y) = e^{-f_x \frac{x}{2}} & \left[\int_0^L dx' e^{-f_x \frac{x'}{2}} \int_0^{D\pi} dy' \left[1 - \theta \left(\sigma - D \left| \sin \frac{y'}{D} \right| \right) \right] \psi_k(x', y') \right. \\ & \left. + \int_L^\infty dx' e^{-f_x \frac{x'}{2}} \int_0^{D\pi} dy' \psi_k(x', y') \right], \end{aligned} \quad (19)$$

while in case $x \leq L$ (it follows that $\theta(L - x) = 1$) Eq. (7) is reduced to

$$\begin{aligned} \lambda_k \psi_k(x, y) = & \left[1 - \theta \left(\sigma - D \left| \sin \frac{y}{D} \right| \right) \right] e^{-f_x \frac{x}{2}} \times \\ & \left[\int_{L-x}^L dx' e^{-f_x \frac{x'}{2}} \int_0^{D\pi} dy' \left[1 - \theta \left(\sigma - D \left| \sin \frac{y'}{D} \right| \right) \right] \psi_k(x', y') \right. \\ & \left. + \int_L^\infty dx' e^{-f_x \frac{x'}{2}} \int_0^{D\pi} dy' \psi_k(x', y') \right] \end{aligned} \quad (20)$$

The lower bound of the first integral is $L - x$ instead of 0 because three particles can not be closer than L , i.e. $x + x' \geq L$, when the channel is narrow, $D < 2\sigma/\sqrt{3}$.

If $D |\sin(y/D)| > \sigma$, one can see that the r.h.s of Eq. (20) in the $x \rightarrow L - 0$ limit is the same as the r.h.s of Eq. (19) in the $x \rightarrow L + 0$ limit, i.e. ψ is continuous at $x = \sigma$. Moreover, the integrals in Eq. (20) do not depend on y , and in Eq. (19) do not depend neither on x

nor y . Therefore we conclude that the eigenfunctions have to be in the following form,

$$\psi_k(x, y) = \begin{cases} [1 - \theta(\sigma - D |\sin(y/D)|)] \varphi_k(x) & \text{if } x \leq L \\ e^{-f_x \frac{x-L}{2}} \varphi_k(L) & \text{if } x > L \end{cases} \quad (21)$$

Substituting these forms into Eq. (20) the y' integrals can be performed and we can see that $\varphi_k(x)$ is determined by the following eigenvalue equation:

$$\lambda_k \varphi_k(x) = D\pi e^{-f_x \frac{x}{2}} \left(\frac{e^{-f_x \frac{L}{2}}}{f_x} \varphi_k(L) + \varepsilon \int_{L-x}^L dx' e^{-f_x \frac{x'}{2}} \varphi_k(x') \right) \quad (22)$$

where we used the notation

$$\varepsilon = 1 - \frac{2}{\pi} \arcsin \frac{\sigma}{D} \quad (23)$$

Differentiating Eq. (22) with respect to x and substituting into itself we obtain the following differential equation:

$$\varphi_k''(x) - (f_x \alpha_k)^2 \varphi_k(x) = 0 \quad (24)$$

where

$$\alpha_k^2 = \frac{1}{4} - \left(\frac{D\pi\varepsilon}{f_x \lambda_k} e^{-f_x \frac{L}{2}} \right)^2 \quad (25)$$

It follows that the solution has the following form:

$$\varphi_k(x) = A_k^+ e^{f_x \alpha_k x} + A_k^- e^{-f_x \alpha_k x}. \quad (26)$$

The integration constants A_k^+ and A_k^- can be determined by substituting (26) into (22) obtaining a system of homogeneous linear equations.

$$e^{-f_x \alpha_k L} \left(1 - \frac{\varepsilon}{\frac{1}{2} + \alpha_k} \right) A_k^- + e^{f_x \alpha_k L} \left(1 - \frac{\varepsilon}{\frac{1}{2} - \alpha_k} \right) A_k^+ = 0 \quad (27)$$

$$\lambda_k A_k^- - D\pi\varepsilon \frac{e^{-f_x \frac{L}{2}} e^{f_x \alpha_k L}}{f_x \frac{1}{2} - \alpha_k} A_k^+ = 0 \quad (28)$$

The requirements of the nontrivial solution is that the determinants of the 2 by 2 matrix of the coefficients has to be zero. It gives the eigenvalues of the transfer operator through the following equation

$$\tanh(f_x \alpha_k L) = 2\alpha_k \frac{\left(\frac{1}{4} - \alpha_k^2\right) - \varepsilon^2}{\left(\frac{1}{4} - \alpha_k^2\right) (1 - 4\varepsilon) + \varepsilon^2} \quad (29)$$

However, this exactly corresponds to Eq. (3.25) of Ref. [60], but the eigenfunction is different.

From Eq. (25) and (28) we get that

$$\frac{A_k^+}{A_k^-} = e^{-f_x \alpha_k L} \sqrt{\frac{\frac{1}{2} - \alpha_k}{\frac{1}{2} + \alpha_k}} \quad (30)$$

therefore the eigenfunction can be written as

$$\varphi_k(x) = A_k^- \left(e^{-f_x \alpha_k x} + e^{f_x \alpha_k (x-L)} \sqrt{\frac{\frac{1}{2} - \alpha_k}{\frac{1}{2} + \alpha_k}} \right) \quad (31)$$

where A_k^- is only a normalization constant.

The eigenvalues can be expressed from Eq. (25) as follows

$$\lambda_k = D\pi\varepsilon \frac{e^{-f_x \frac{L}{2}}}{f_x} \frac{1}{\sqrt{\frac{1}{4} - \alpha_k^2}}, \quad (32)$$

therefore Eq. (29) determines all the eigenvalues of the transfer operator, and Eq. (31) gives the corresponding eigenfunctions in case when $\lambda_k \neq 0$. We can also get the expectation values and the correlation functions of any quantity which depends only on the relative positions of the nearest neighbour particles, see Eq. (12). To understand its special behaviour, we examine the solutions of Eq. (29) in detail.

The r.h.s. of Eq. (29), as a function of α , reaches a local maximum at $\alpha = 1/2 - \varepsilon$, where it is 1, and it is zero at $\alpha = \sqrt{1/4 - \varepsilon^2}$, see Fig. 2. Furthermore between these

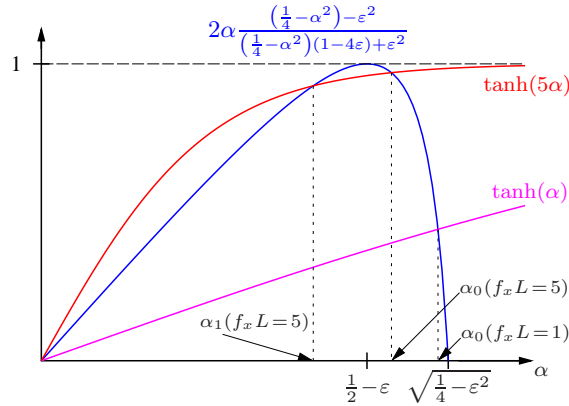


FIG. 2. An exemplification of the real solutions of Eq.(29) for $D^* = 1.015$ (i.e. $\varepsilon \approx 0.1096$). We have $\alpha_0 = \sqrt{1/4 - \varepsilon^2}$ when $f_x = 0$, moreover α_0 is a monotonic decreasing function of f_x and its value goes to $1/2 - \varepsilon$ as f_x approaches infinity. There is only one real solution, α_0 , when $f_x L < \frac{2+4\varepsilon}{1-2\varepsilon}$, and there are two different ones, α_0 and α_1 , in other cases. The value of α_1 also goes to $1/2 - \varepsilon$ as f_x approaches infinity.

points it is monotonically decreasing function, therefore Eq. (29) have a unique root, α_0 , in the interval $[1/2 - \varepsilon, \sqrt{1/4 - \varepsilon^2}]$, and α_0 is monotonic decreasing function of f_x with

$\lim_{f_x \rightarrow 0} \alpha_0 = \sqrt{1/4 - \varepsilon^2}$ and $\lim_{f_x \rightarrow \infty} \alpha_0 = 1/2 - \varepsilon$. It is easy to see that α_0 gives the largest eigenvalue, because λ is a monotonic increasing function of α^2 and the r.h.s. of Eq. (29) is negative or greater than 1 for $\alpha > \sqrt{1/4 - \varepsilon^2}$. Moreover, the $\alpha < 0$ solutions give the same eigenvalues and eigenvectors as the positive ones, thus the proper real solutions are in the $[0, \sqrt{1/4 - \varepsilon^2}]$ interval. Below $1/2 - \varepsilon$ there is another real solution, α_1 , when $f_x L \geq (2 + 4\varepsilon)/(1 - 2\varepsilon)$. This corresponds to the second largest eigenvalue, λ_1 , and α_1 has the same high axial force limit as α_0 has, i.e. $\lim_{f_x \rightarrow \infty} \alpha_1 = 1/2 - \varepsilon$. All the other solutions of Eq. (29) give imaginary α_k , and they correspond to other smaller eigenvalues, which are real because only α_k^2 is involved in Eq. (32). We note that α_1 is imaginary, too, for $f_x L < (2 + 4\varepsilon)/(1 - 2\varepsilon)$, but α_1^2 , and so λ_1 is analytic function of the dimensionless axial force at $f_x L = (2 + 4\varepsilon)/(1 - 2\varepsilon)$, too.

The transcendental equation (29) does not have closed-form solutions, however, for further studies of the one row–two row layering transition we can derive an approximate solution which can be handled easily. We are motivated from two sides. On the one hand getting analytic formulas is useful to study the limiting behaviour, on the other hand, the numerically precise solution of (29) is difficult, because α_0 changes its value in a very narrow interval, so when $D \rightarrow \sigma$, (i.e. $\varepsilon \rightarrow 0$) one needs high precision for α_0 . Also in Ref. [60] the authors give approximate solutions for low and high pressures (i.e. axial forces), which are based on the series expansion of the tanh function, thus neither the small nor the large f_x approximations can describe the most interesting intermediate axial force regime when the system changes its behaviour from a one-row to two-row layering. To go beyond their results, here we show a more efficient approximation.

Just the difficulty of the numerical solution of our problem gives the key for the analytic approximation. We know that $\alpha_0 \in [1/2 - \varepsilon, \sqrt{1/4 - \varepsilon^2}]$, therefore $\alpha_0 \approx 1/2$ for arbitrary axial force when D approaches to σ from above ($\varepsilon \rightarrow 0$). Therefore we can use the approximation $\tanh(f_x \alpha_0 L) \approx \tanh(f_x L/2)$. Moreover, we know that $\lim_{f_x \rightarrow \infty} \alpha_1 = 1/2 - \varepsilon$, therefore, at least in the high axial force limit, also the $\tanh(f_x \alpha_1 L) \approx \tanh(f_x L/2)$ approximation is valid. As D goes to σ these approximations are better for arbitrary value of f_x . However, for very small f_x this is not a good approximation. But that is clearly the ideal gas limit which is not very interesting. What is important, that our approximation is quite good for well above $D = \sigma$ when f_x is large and very good for low f_x , too, in case when $D \gtrsim \sigma$. Therefore it is not necessary to use series expansion for the tanh function, because

we get a cubic equation for α . The roots of this cubic equation can be used to study the behaviour of the system in a very wide f_x range except the ideal gas limit.

Nevertheless, we can do further reliable approximations to get analytical formulas which are more manageable than the roots of a cubic equation. The r.h.s. of Eq. (29), and also its derivatives change very rapidly with α , therefore it can not be approximated by a single low order polynomial, but the nominator and the denominator are simple second order polynomials which change their values slowly, therefore we can use first order approximations for them. As we are interested mainly in the high f_x behaviour, we use a series expansion around $1/2 - \varepsilon$ both in the numenator and the denominator. We obtain the following quadratic equation in α ,

$$\tanh \frac{f_x L}{2} = 2\alpha_{0,1} \frac{1 - 2\alpha_{0,1}}{(1 - 2\varepsilon)^2 - (1 - 4\varepsilon)2\alpha_{0,1}}. \quad (33)$$

The solution of this equation for α can be written as

$$\alpha_{0,1} = \frac{\varepsilon + (\frac{1}{2} - \varepsilon)e^{f_x L} \pm \sqrt{\frac{1}{4} + (e^{f_x L} - 1)\varepsilon(1 - 2\varepsilon)}}{e^{f_x L} + 1}. \quad (34)$$

From this equation we get the limits

$$\alpha_{0,1} \approx \frac{1}{2} - \varepsilon \pm \sqrt{\varepsilon} e^{-f_x \frac{L}{2}} \approx \frac{1}{2} - \varepsilon \quad (35)$$

when $2\varepsilon e^{f_x L} \gg 1$ and

$$\alpha_0 \approx \frac{1}{2} - \varepsilon^2 e^{f_x L} - \frac{e^{-2f_x L}}{2} \approx \sqrt{\frac{1}{4} - \varepsilon^2 e^{f_x L}} \quad (36)$$

when $2\varepsilon e^{f_x L} \ll 1$. Finally, the last approximation in Eq.(36) is valid when $2\varepsilon^2 \gg e^{-3f_x L}$. Eq. (36) is not valid for α_1 because it is far from $1/2 - \varepsilon$ at low axial force. Moreover, it is certainly neither valid for α_0 when f_x is very low, because in our derivation we supposed at the beginning that we are far from the ideal gas limit. The case when $f_x L \approx -\ln(2\varepsilon)$ defines a special range, where neither Eq. (35) nor Eq. (36) can be applied, however Eq. (34) can be used.

IV. RESULTS

In this section we first present our TOM results for hard spheres and show that the close packing zigzag structure develops continuously with increasing density (force). After

this, the packing of hard cylinders is examined, where a layering structural change emerges between one-row and two-row fluids. The relations of these systems with the well-known 1d hard rod fluid is also considered as these systems become 1d in extreme confining diameters. In the case of hard spheres $D = 0$ corresponds to the 1d limit, while the hard cylinders exhibit this behaviour in the range of $0 < D < \sigma$. The results of Tonks [65] can be summarized in such narrow pores as follows: 1) there is no fluid-solid phase transition as the system is one-dimensional with short-range interactions; 2) the equation of state can be written down with $f_x = \rho/(1 - \rho/\rho_{cp})$ (it is called Tonks equations) in the whole range of density, where ρ_{cp} is the close packing density; and 3) the nearest neighbour probability distribution function is decaying exponentially with the distance of the neighbors, i.e. $f(x) = \theta(x - l)f(l)e^{-f_x(x-l)}$, where l is the length of the hard rod [64]. Now we continue with presenting our exact results in wider pores, where the following dimensionless quantities are used: 1) $x^* = x/\sigma$, $y^* = y/\sigma$, $D^* = D/\sigma$, $f_x^* = f_x\sigma$, $\rho^* = \rho\sigma$ for spheres, and 2) $x^* = x/L$, $D^* = D/\sigma$, $f_x^* = f_xL$, $\rho^* = \rho L$ and $\kappa_T^* = \kappa_T/(\beta L)$ for cylinders.

A. Hard spheres on the surface of cylindrical tube

Our results are presented for $0 < D^* < \sqrt{3}/2$, where only first neighbour interactions are present and zigzag structure develops with the increasing density. Note that our formalism using the kernel from Eq.(5) with Eq.(14) remains also valid in wider pores of $\sqrt{3}/2 < D^* < 1$. However, we leave this range for future studies, because the situation can be much more complicated as chiral structures compete with zigzag structures in the vicinity of close packing [27, 29] and analytic solutions cannot be derived from TOM. In Fig. 3 we show the equation of state of hard spheres at different pore diameters from zero to close packing densities. There are two reasons why the shape of the curve is changing with D : 1) the close packing density increases with D as follows: $\rho_{cp} = (\sigma^2 - D^2)^{-1/2}$, and 2) it can be shown analytically that $f_x = 3/2 \rho/(1 - \rho/\rho_{cp})$ for $D \neq 0$ in high axial force limit instead of Tonks equation, which is valid only for $D = 0$. We show the relative error $(1 - f_x^{\text{approx.}}/f_x)$ of the above equation and the Tonks equation as a function of density in the inset of Fig. 3 for $D^* = \sqrt{3}/2$. One can see that the Tonks equation is better at low densities, while the high axial force limiting equation becomes quite accurate for $\rho^* > 1$. At intermediate densities ($0.5 < \rho^* < 1$) both equations are inaccurate with about 20–30% error. This shows that the

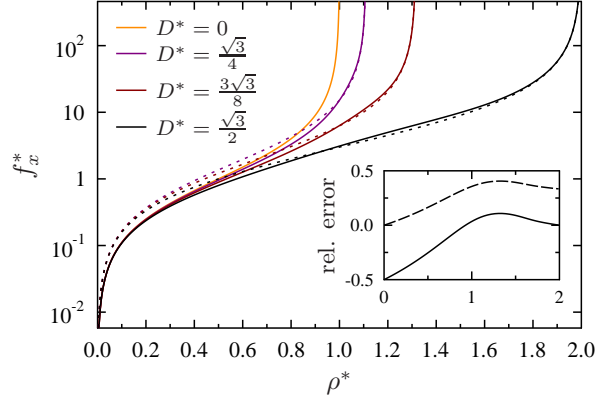


FIG. 3. The equation of state (dimensionless axial force vs. 1d density) of the spheres confined into a cylindrical surface is shown at different pore diameters. Continuous curves corresponds to the exact results, while the dashed ones is obtained in the high axial force limit. The dashed and the continuous curves are identical at $D = 0$. The deviation of the equation of state from the Tonks equation (dashed curve) and from the equation of high f_x limit (continuous curve) is shown for the widest pore in the inset.

equation of state cannot be written down with a simple Tonks-type equation in the whole range of density. The simple reason for this is that the system of hard spheres undergoes a change from a fluid-like to a zigzag-like structure. The $\frac{3}{2}$ prefactor of the equation of state is the consequence of zigzag arrangement because x and y coordinates couple in such structures. The axial and circular nearest neighbor probability distribution function, which are obtained from Eqs.(10,11), justifies the gradual structural change with increasing axial force (density) (see Fig. 4). At intermediate densities (see the curve for $f_x^* = 1$) one can see that $f(x)$ has only one maximum at $x^* = 1$ and decays exponentially as it happens in the case of Tonks gas. However, the fact that $f(x) > 0$ in the interval of $1/2 < x^* < 1$ shows that there are some neighbors with $x^* < 1$ distance and these particles must form zigzag dimer. The structure of $f(y)$ also confirms this, as it has a peak when the neighbors are at the opposite side of the pore ($y = D\pi/2$). At higher densities the structure of the system substantially deviates from that of 1d rods as $f(x)$ becomes two-peaked (see the curve for $f_x^* = 3$): one peak at $x^* = 1$ is the remainder of the 1d hard rod structure, while the second one at $x^* < 1$ is due to the emergence of zigzag clustering. At this density the structure of the system is mixture of fluid and zigzag clusters. At higher densities (see the curve for

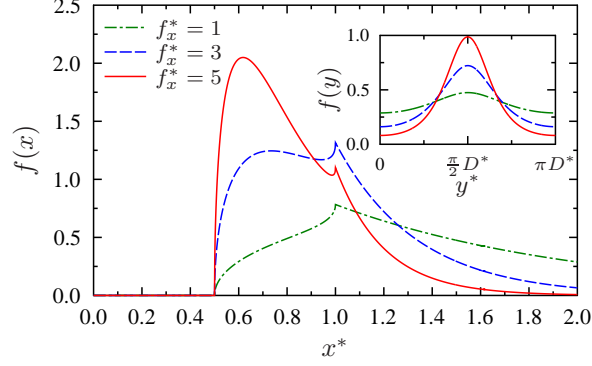


FIG. 4. Nearest neighbor axial and circular distribution functions for the spheres confined into a cylindrical surface are shown for different axial forces at $D = \sqrt{3}\sigma/2$. Axial distribution ($f(x)$) vs. nearest neighbor axial distance (x) in the main figure, while circular distribution ($f(y)$) vs. nearest neighbor circular distance (y) in the inset.

$f_x^* = 5$) the majority of the particles get into the zigzag cluster, while the fluid-like structure is suppressed as $f(x^* = 1)$ decreases. At the close packing limit ($f_x \rightarrow \infty$), only one peak survives in $f(x)$ at $x^* = 1/2$, while $f(x^* = 1)$ vanishes. It is also interesting to consider the fraction of neighbors inside the border of $x^* = 1$, which is defined as $X_{x<\sigma} = \int_0^\sigma f(x)dx$ (see Fig. 5). This serves information about the extent of zigzag structure as it is zero in the

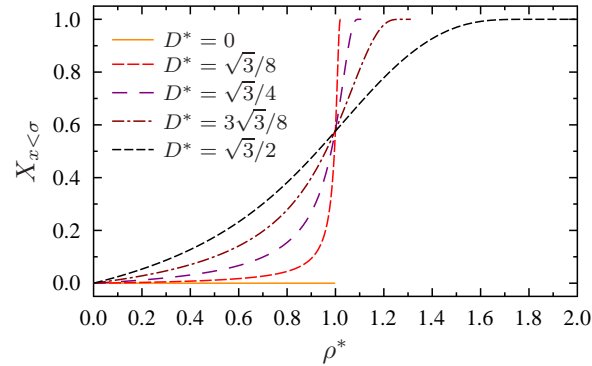


FIG. 5. Fraction of nearest neighbors within the axial distance $x < \sigma$ vs. 1d density for different pore diameters.

perfect fluid (1d Tonks gas), while it is one in the perfect zigzag structure. Apart from the trivial $D = 0$ limit (corresponding to the system of 1d hard rods), $X_{x<\sigma} \rightarrow 1$ at the high density limit for any D . This proves that the TOM accounts for the close packing structure of hard spheres at the infinite axial force. It is an interesting feature of confined hard spheres

that $\rho = 1$ is a dividing line for all values of D , because this is the maximum value of density at which the formation of a straight chain of hard spheres is still possible. Fig. 5 also shows that the formation of zigzag clusters starts at lower densities, while the saturation occurs at higher densities with increasing pore diameter. Finally we note that the integral equation theory predicts similar trends in wider pores, as the positional ordering of hard spheres is anisotropic on the outer surface of cylindrical pores, too [66].

B. Hard cylinders on the surface of cylindrical tube

The examined range of pore diameters can be divided into two regions: 1) if $0 < D^* < 1$, only a row of hard cylinders can form and 2) if $1 < D^* < \sqrt{2}/3$, two rows of cylinders are allowed to form because two hard cylinders can be located at the same axial position, x . The first case corresponds to the well-known 1d hard rod fluid even if the particles are allowed to move on the circle with radius D , because the axial contact distance is always L . Therefore one may expect that the 1d hard rod nature survives in a pore with $D^* = 1 + 10^{-\epsilon}$, where $\epsilon \rightarrow \infty$, while two rows develop continuously in the possible widest pore ($D^* = 2/\sqrt{3}$). To see the difference between the two limiting cases, where maximum two rows are allowed to form, we present the equation of state at some values of D^* in Fig. 6. One can see that

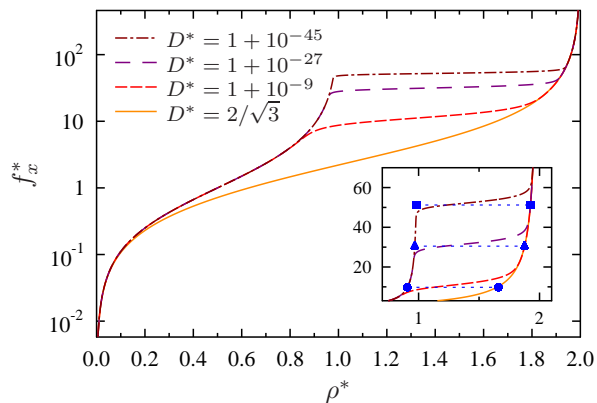
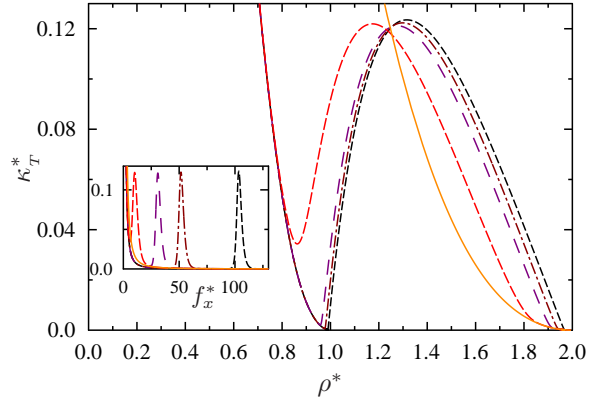


FIG. 6. Equation of state of oriented hard cylinders in a cylindrical pore at different pore diameters. The main figure is made in log-lin scale, while the inset in lin-lin scale. The horizontal blue lines correspond to the one-row to two-row transition force, $f_x^* = -\ln 2\epsilon$. Symbols at the end of these lines denote the densities coming from the low end high axial force approximations according to Eq. (35) and Eq. (36).

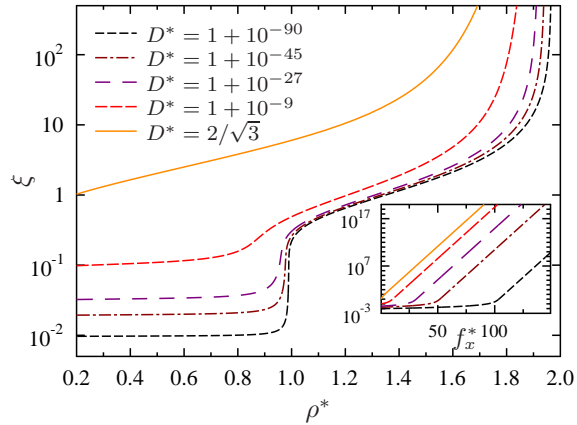
all curves converge to the close packing density of two-row structure, $\rho_{cp}^{(2)}$, which is given by $\rho_{cp}^{(2)} = 2/L$. In addition to this, from Eq.(35) it immediately follows that the equation of state is given by $f_x = \rho/(1 - \rho/\rho_{cp}^{(2)})$ in the high axial force limit, which is independent from the pore diameter. These results indicate that the high density structure consists of two rows, where the Tonks equation of 1d hard rods is also valid with the appropriate close packing density $\rho_{cp}^{(2)}$. The reason why the Tonks equation is valid is that there is no coupling between x and y coordinates of the hard cylinders, which is not the case in the zigzag structure of hard spheres. One can also see that the hard cylinders behave very differently at intermediate densities for pore diameters very close to the lower limit of $D^* = 1$. This manifest in a very steep equation of state at the vicinity of the axial force $f_x^* = -\ln 2\varepsilon$, where the density suddenly changes almost from $\rho_{cp}^{(1)}$ to $\rho_{cp}^{(2)}$. Here $\rho_{cp}^{(1)} = 1/L$ denotes the close packing density of one row fluid. Below this density, as follows from Eq.(36), the equation of states can be well approximated by the Tonks equation $f_x = \rho/(1 - \rho/\rho_{cp}^{(1)})$. From these results it is clear that one row of hard cylinders transforms into two rows of them in a narrow window of axial force as can be seen in Fig. 6.

The border between the validity of the high and low force approximations, Eqs.(35) and (36), respectively, is given by $f_x^* = -\ln(2\varepsilon)$. The layering cross-over between one-row and two-row structures happens at this point. We mention here, that the behaviour of the system at this axial force can be approximated as a first order transition if the connecting terms in the kernel of the transfer operator is omitted. In this approximation the transfer operator is not a positive operator, therefore the phase transition cannot be excluded anymore [48]. The Gibbs free energy of one row fluid becomes identical with that of 1d rods, while that of two-row fluid is approximated using the high axial force limit of α , see Eq.(35). Equating the Gibbs freeenergies ensures the equality of chemical potentials and provides the transition pressures, which gives exactly the border between the above low and high f_x approximations, $f_x^* = -\ln(2\varepsilon)$. At this axial force it is easy to determine the coexisting densities of the fluids from the corresponding equation of states. We show these pairs of densities in the inset of Fig. 6 with blue markers. This inset shows the equation of state in linear scale. It can be seen that the transition is shifted upwards according to $f_x^* = -\ln 2\varepsilon$ as $D \rightarrow 2$. However, there is no genuine phase transition in the system, the exact analytic curves show that the equation of state is very flat in this region. Therefore it is interesting to examine the behaviour of the isothermal compressibility, $\kappa_T := -\frac{1}{L_x} \frac{\partial L_x}{\partial f_x} = -\rho \frac{\partial^2(\beta g)}{\partial f_x^2}$ and the correlation length,

$\xi^{-1} = -\ln(\lambda_1/\lambda_0)$ which can be determined using Eq. (34). The curves of the resulting lengthy formulas are shown in Fig. 7. The compressibility curve, see Fig. 7(a), has a bump at the transition but the height of this bump is constant. Here we have no divergence,



(a)



(b)

FIG. 7. (a) Dimensionless isothermal compressibility as a function of density for several pore diameters. (b) Correlation length as a function of density. The insets show the same as the main figures as a function of axial force. The color code of the curves are shown in (b).

which is in contrast with some other q1d systems, where real critical divergences occur as some geometrical parameters approach to a special critical value and the axial force goes to infinity, see e.g. Ref. [63]. Interesting to see that in the close packing limit of the one-row structure the system is very rigid, the compressibility becomes very small. The behaviour of the correlation length also supports the aboves. Below the structural change the correlations are very weak and the correlation length is almost zero, see Fig 7(b). This behaviour is very

similar to that of spheres because the nearest neighbour interactions dominate the behaviour of the system in the case of one-row structure, while the next-nearest neighbour interactions hardly play any role. However the correlation length starts to diverge exponentially with the axial force as the two-row structure builds up at the structural transition. We can show using Eq. (35) that $\xi \approx \sqrt{\varepsilon e^{f_x^*}}$ above the transition, but there is no any peak in ξ at the transition. Here we note that in a very recent manuscript, Ref. [67], Hu et. al. propose that a sudden structural change without genuine phase transition, like the one row–two row layering transition in our case, can be associated with eigenvalue crossing or splitting of the transfer operator. The largest eigenvalue is certainly analytic, guaranteed by the Perron–Frobenius–Jentzsch theorem, but the second and third or any other eigenvalues can cross each other, causing a non-smooth or non-monotonic behaviour of the correlation length. Regarding this context we mention that this is not the case in our model. All the eigenvalues can be given by Eq.(32) where α_k are determined by Eq.(29). We have seen that Eq.(29) has at most two real solutions, which can not cross each other, and examining all the imaginary solutions we find that neither of them can cross each other, therefore that is also true for all the eigenvalues.

The axial nearest neighbour distribution confirms the predictions coming from the above analysis, which is shown in wide and narrow pores in Fig. 8. In the possible widest pore,

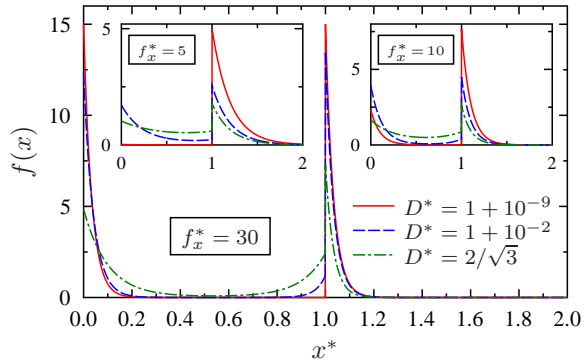


FIG. 8. Nearest neighbor axial distribution function as a function of axial distance at different axial forces.

$D^* = 2/\sqrt{3}$, it can be seen that the occupation of the space happens in a way that one-row structure does not exist even at very low densities and the close packing structure with two rows develops continuously with increasing f_x . In very narrow pores, $f(x)$ carries the

feature of 1d hard rods as it is zero for $x < L$ and decays exponentially for large distances. Therefore hard cylinders form only one row at low and middle densities (see the inset of Fig. 8 at $f_x^* = 5$). However, $f(x)$ becomes peaked at $x = 0$ even in the narrowest pores at very high axial forces, which proves that the two-row structure develops in narrow and wide pores, too. It can be also seen that the peaks of $f(x)$ at $x = 0$ and $x = L$ becomes sharper and narrower with increasing f_x (or density), which is reminiscence of solid structures. Further information can be gained from the fraction of nearest neighbours (X) being in the different regions of the axial distance. These regions are the followings: $0 < x < L/2$, $L/2 < x < L$ and $L < x < \infty$. We show $X_{0 < x < L/2}$, $X_{L/2 < x < L}$ and $X_{L < x}$ as a function of density for narrow and wide pores in Fig. 9. In narrow pore $X_{L < x}$ is almost one up to about $0.9\rho_{cp}^{(1)}$, while the

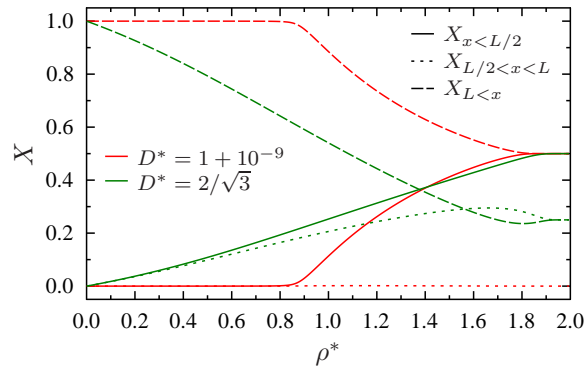


FIG. 9. Fraction of nearest neighbors at different regions of the axial distance between the neighbors vs. one-dimensional density for different pore diameters.

other two are approximately zero. This is in agreement with our previous statements that the particles form a single row and behaves as a 1d hard rod fluid. At the close packing density, one gets that $X_{0 < x < L/2} = 1/2$, $X_{L < x} = 1/2$, while $X_{L/2 < x < L} = 0$. This shows that the first right neighbour of a given particle can be either located at the same axial position above it or at the distance $x = L$ with equal probability as $f(x)$ becomes delta function at the close packing. This suggests that two particles at the same axial position form a dimer and the system form a layered structure along the axial direction resembling a smectic-like configuration. In wide pore, $D^* = 2/\sqrt{3}$, 1d hard rod fluid does not exist as $X_{L < x}$ is one only in the ideal gas limit. The monotonically increasing feature of $X_{0 < x < L/2}$ and $X_{L/2 < x < L}$ supports the idea that two rows develop continuously. As $X_{0 < x < L/2} = 1/2$, $X_{L/2 < x < L} = 1/4$ and $X_{L < x} = 1/4$ at the close packing density, the 50% of the first neighbours can be found at

the same axial position as before, but only 25% of the particles is outside of the axial overlap region. This indicates that the first neighbours do not form a pair and the structure is not layered at the close packing density, resembling a columnar-like configuration of particles. From these results the close packing structure can not be identified with a solid.

Finally, we touch upon the question of the relation of our results with others coming from density functional theories such as fundamental measure theory (FMT). If $D^* < 1$ then the FMT-based density functionals (DF) recovers the exact Percus density functional for hard rods [61]. If $D^* > 1$, which allows two particles pass each other, the DF is not exact. However it can be applied, by imposing appropriate periodic boundary conditions, to study configurations of particles with density profile varying along the circular axes while it is constant along the cylinder axis. As the mean density of particles increases the system exhibits a second order fluid-columnar phase transition with the transition density not depending on D and equal to that of the bulk. Note that at bulk the smectic and columnar phases of hard squares are identical. For certain values of D as the density increases first order transitions between columnar phases with different number of columns take place with transition densities strongly depending on D .

However if we impose the density profile to be constant along the circular axes and non-uniform along the axis of cylinder the system is completely equivalent to a bulk fluid. It is clear that an extra condition, reflecting the finiteness of the system along the transverse direction, should be imposed. The way it can be implemented is not clear for us. The unique recipe at the level of the grand-canonical one-body density based DF is to allow the density to increase up to its maximum close-packing value, calculated by taking into account that only two particles can fit inside the pore. But if we implement this recipe we obtain the same smectic free-energy branch as that of the bulk fluid. Thus the second order fluid-smectic transition only takes place if its bulk value fall below the maximum allowed close-packing density and in this case the free-energy is always bellow that corresponding to the columnar except at the bifurcation point.

Finally if we leave the density profile to vary along both transversal and axial directions we find a crystalline phase as a local minimum of the DF. Its relative stability with respect to the columnar phase strongly depends on packing fraction and D . The crystalline phase on the cylinder can even be more stable than the smectic only for narrow packing fraction intervals usually located at high densities where a good commensuration between the bulk

crystal lattice parameter and the perimeter of cylinder exists.

In any case if the transition to the smectic finally occurs the density profile will be independent on the cylinder radius which constitutes a strong drawback of the grand-canonical one-body density based DF formalism. Note that if a two-body density based DF would be available then the two-body density profile would reflect the effect of the system finiteness along the perimeter has on transverse particle correlations despite the unchanged value of the density profile along the perimeter. On lattice systems this kind of DF has been worked out [68–70], so it is mandatory its extension to the continuum. A promising route to take into account the finiteness of the system along one spatial direction at the level of one-body density based DF could consist on the extension of the formalism developed in Ref. [71] to obtain a canonical version of DF for finite systems from the grand canonical one.

V. CONCLUSIONS

We have reformulated the transfer operator method of Percus and Zhang [60] to obtain some additional information about the thermodynamic properties and the structure of quasi-one-dimensional hard body fluids. Our method is based on the special grouping of pair interactions to obtain the isochoric–isobaric partition function as operator products of the transfer operator. In the thermodynamic limit ($N \rightarrow \infty$) the largest eigenvalue of the transfer operator is the most dominant and provides the Gibbs free energy, while the corresponding eigenfunction gives information about the local structure, because we use a symmetric form of the transfer operator. To give an explicit analytic solution, we devised an efficient approximation, thus we were able to handle the case when the pore is just as wide to allow the accommodation of two particles at the same axial position. Our method can be applied only for hard particles in cylindrical confinements and stripes with periodic boundary conditions where only first and second neighbour interactions are present.

Using our method, we have examined the ordering behaviour of the monolayer of hard bodies, which are adsorbed on the surface of the hard cylindrical pore. In the case of hard spheres, which are adsorbed on the inner surface of the channels, we could perform analytic calculations up to pore diameter $W = (1 + \sqrt{3}/2)\sigma$, which is the upper limit of the first neighbor interactions. It is found that the phase behavior of confined hard spheres deviates substantially from the strictly 1d case, which corresponds to $W = \sigma$. This manifests in the

formation of zigzag-like structure at high density which can be seen in the distribution of first neighbors and the equation of state in the vicinity of the close packing density, ρ_{cp} .

This latter one obeys

$$f_x = \frac{3}{2} \frac{\rho}{1 - \rho/\rho_{cp}}, \quad (37)$$

which is different in a factor of one and half from the well-known Tonks's equation of the 1d hard rods, $f_x = \rho/(1 - \rho/\rho_{cp})$. The emergence of the extra one and half factor is due to the coupling of axial and circular freedoms in the zigzag structure. Nevertheless, Eq. (37) differs also from the high f_x limiting equation of state of hard disks in narrow stripe derived by Godfrey and Moore in Ref. [53]. In their case there is a prefactor two instead of one and half like in the case of periodic boundary condition. As shown in Sec. IIIA this is related to the smooth behaviour of the x projection of the contact distance in the vicinity of its minimum value. This shows that the confined hard spheres cannot be mapped onto a system of hard disks in a periodic narrow stripe. Regarding the hard cylinders, which are also adsorbed on the inner surface of the tubular pore, we have found that the Tonks's equation of state is exact for $\sigma < W < 2\sigma$, because the particles are not allowed to pass each other in the tube and only first neighbor interactions are present. In wider pores $2\sigma < W < (1 + 2/\sqrt{3})\sigma$, a structural change from one-row fluid to two-row fluid is observed as the particles are allowed to pass each other. This layering change becomes sharper as the pore diameter is decreased to the lower limit (2σ), because there is less and less room to form the second row. Interestingly, the equation of state of one-row fluid and that of two-row one can be described with the Tonks's equation, where the corresponding one-row and two-row close packing densities has to be used. Here, the factor of one and half is missing because there is no coupling between axial and circular freedoms. We have shown that the layering can be seen as a virtual 1st order transition using the Gibbs free energies of the purely one-row and two-row structures. The lack of true phase transition is due to the connecting terms of the transfer operator. Therefore it is possible that even simulation studies find this layering change to be of 1st order for pore diameter $W = 2\sigma + \epsilon$, where $\epsilon \rightarrow 0$. However, simulation studies can not be implemented for such pore diameters. We have found that the local structure resembles the solid phase as $W \rightarrow (1 + 2/\sqrt{3})\sigma$, while it is smectic-like for $W = 2\sigma + \epsilon$, where $\epsilon \rightarrow 0$.

There are two important reasons to use exact methods for systems with dimensional restrictions between one and two dimensions. First, present-day classical density functional

theories (DFT) are wrong for quasi-one-dimensional systems, because they predict that the phase behavior of cylindrically confined hard cylinders is identical to that of the two-dimensional bulk system for smectic-like configurations. In addition, DFT predicts phase transitions from the fluid to the smectic or columnar phases, between columnar phases with different number of columns, and finally to the crystalline phase. The relative stability between different phases depends on density and pore width. Some of these phase transitions occur for $2\sigma < W < (1 + 2/\sqrt{3})\sigma$ [61, 62]. The failure of DFT can also be present for other particle shapes if particles are constrained on the surface of a cylinder or they move on a periodic narrow surface. These unphysical results are ultimately due to the unrealistic representation of anisotropic correlations in the absence of symmetry-breaking external fields [69, 70]. Second, even molecular dynamics and Monte Carlo simulations can predict 1st order phase transitions in q1d systems such as hard spheres embedded into a cylindrical pore, where the possibility of a phase transition can be excluded with complete certainty [48]. This failure of the simulations can be attributed to the poor sampling of the configuration space and to the presence of vast amounts of jammed and glassy states. To check the reliability of DFT and simulation studies it would be useful to extend the transfer operator method for wider pores.

ACKNOWLEDGMENTS

P.G. and S.V. would like to acknowledge the financial support of the National Research, Development, and Innovation Office (NKFIH K124353). Financial support under grants FIS2015-66523-P and FIS2013-47350-C5-1-R from Ministerio de Economía y Competitividad (MINECO) of Spain is acknowledged.

-
- [1] L. D. Gelb, K. E. Gubbins, R. Radhakrishnan, and M. Sliwinska-Bartkowiak, *Rep. Prog. Phys.* **63**, 727 (2000).
 - [2] K. Koga, G. T. Gao, H. Tanaka, and X. C. Zeng, *Nature* **412**, 802 (2001).
 - [3] K. Koga and H. Tanaka, *J. Chem. Phys.* **124**, 131103 (2006).
 - [4] H. Löwen, *J. Phys.: Condens. Matter* **21**, 474203 (2009).
 - [5] S. S. Ashwin and R. K. Bowles, *Phys. Rev. Lett.* **102**, 235701 (2009).

- [6] T. Franosch, S. Lang, and R. Schilling, *Phys. Rev. Lett.* **109**, 240601 (2012).
- [7] S. S. Ashwin, M. Z. Yamchi, and R. K. Bowles, *Phys. Rev. Lett.* **110**, 145701 (2013).
- [8] S. Lang, T. Franosch, and R. Schilling, *J. Chem. Phys.* **140**, 104506 (2014).
- [9] H. H. Wensink, H. Löwen, M. Marechal, A. Hrtel, R. Wittkowski, U. Zimmermann, A. Kaiser, and A. M. Menzel, *Eur. Phys. J. Special Topics* **222**, 3023 (2013).
- [10] A. B. G. M. Leferink op Reinink, E. van den Pol, A. V. Petukhov, G. J. Vroege, and H. N. W. Lekkerkerker, *Eur. Phys. J. Special Topics* **222**, 3053 (2013).
- [11] P. Huber, *J. Phys.: Condens. Matter* **27**, 103102 (2015).
- [12] T. Geigenfeind, S. Rosenzweig, M. Schmidt, and D. de las Heras, *J. Chem. Phys.* **142**, 174701 (2015).
- [13] J. F. Robinson, M. J. Godfrey, and M. A. Moore, *Phys. Rev. E* **93**, 032101 (2016).
- [14] Q.-Y. Wu, W.-d. Tian, and Y.-q. Ma, *The J. Phys. Chem. B* **121**, 8984 (2017), pMID: 28863475.
- [15] R. Radhakrishnan, K. E. Gubbins, and M. Sliwinska-Bartkowiak, *Phys. Rev. Lett.* **89**, 076101 (2002).
- [16] M. A. Lohr, A. M. Alsayed, B. G. Chen, Z. Zhang, R. D. Kamien, and A. G. Yodh, *Phys. Rev. E* **81**, 040401 (2010).
- [17] B. Bharti, M. Xue, J. Meissner, V. Cristiglio, and G. H. Findenegg, *J. Am. Chem. Soc.* **134**, 14756 (2012), pMID: 22928969.
- [18] L. Jiang, J. W. J. de Folter, J. Huang, A. P. Philipse, W. K. Kegel, and A. V. Petukhov, *Angew. Chem. Int. Ed.* **52**, 3364 (2013).
- [19] A. Fortini and M. Dijkstra, *J. Phys.: Condens. Matter* **18**, L371 (2006).
- [20] Y. Peng, Z. Wang, A. M. Alsayed, A. G. Yodh, and Y. Han, *Phys. Rev. Lett.* **104**, 205703 (2010).
- [21] M. C. Gordillo, B. Martinez-Haya, and J. M. Romero-Enrique, *J. Chem. Phys.* **125**, 144702 (2006).
- [22] F. J. Duran-Olivencia and M. C. Gordillo, *Phys. Rev. E* **79**, 061111 (2009).
- [23] K. Mochizuki and K. Koga, *PNAS* **112**, 8221 (2015).
- [24] K. Wojciechowski and D. Frenkel, *Comp. Methods in Science and Tech.* **10**, 235 (2004).
- [25] A. Donev, J. Burton, F. H. Stillinger, and S. Torquato, *Phys. Rev. B* **73**, 054109 (2006).
- [26] T. Yue, G. Jiang, and X. Zhang, *Phys. Chem. Chem. Phys.* **13**, 12497 (2011).

- [27] A. Mughal, H. K. Chan, D. Weaire, and S. Hutzler, *Phys. Rev. E* **85**, 051305 (2012).
- [28] M. Z. Yamchi and R. K. Bowles, *Phys. Rev. Lett.* **115**, 025702 (2015).
- [29] L. Fu, W. Steinhardt, H. Zhao, J. E. S. Socolar, and P. Charbonneau, *Soft Matter* **12**, 2505 (2016).
- [30] J. A. Anderson, J. Antonaglia, J. A. Millan, M. Engel, and S. C. Glotzer, *Phys. Rev. X* **7**, 021001 (2017).
- [31] M. Cosentino Lagomarsino, M. Dogterom, and M. Dijkstra, *J. Chem. Phys.* **119**, 3535 (2003).
- [32] C. Grigoriadis, H. Duran, M. Steinhart, M. Kappl, H.-J. Butt, and G. Floudas, *ACS Nano* **5**, 9208 (2011), pMID: 21974835.
- [33] S. Całus, D. Rau, P. Huber, and A. V. Kityk, *Phys. Rev. E* **86**, 021701 (2012).
- [34] H. C. Huang, S. K. Kwak, and J. K. Singh, *J. Chem. Phys.* **130**, 164511 (2009).
- [35] P. Gurin, S. Varga, and G. Odriozola, *Phys. Rev. E* **94**, 050603 (2016).
- [36] L. Fu, C. Bian, C. W. Shields, D. F. Cruz, G. P. Lopez, and P. Charbonneau, *Soft Matter* **13**, 3296 (2017).
- [37] M. R. Khadilkar and F. A. Escobedo, *Soft Matter* **12**, 1506 (2016).
- [38] E. H. Lieb, *Mathematical physics in one dimension: exactly soluble models of interacting particles* (Academic Press, 2013).
- [39] K. Abe and K. Koga, *J. Phys. Soc. Jpn.* **81**, SA021 (2012).
- [40] T. Nath, D. Dhar, and R. Rajesh, *EPL* **114**, 10003 (2016).
- [41] D. Mandal and R. Rajesh, *Phys. Rev. E* **96**, 012140 (2017).
- [42] K. W. Wojciechowski, P. Pieranski, and J. Malecki, *J. Chem. Phys.* **76**, 6170 (1982).
- [43] K. W. Wojciechowski, P. Pieranski, and J. Malecki, *J. Phys. A: Math. Gen.* **16**, 2197 (1983).
- [44] C. Forster, D. Mukamel, and H. A. Posch, *Phys. Rev. E* **69**, 066124 (2004).
- [45] Y. Kantor and M. Kardar, *EPL* **87**, 60002 (2009).
- [46] M. D. Khandkar, R. Stinchcombe, and M. Barma, *Phys. Rev. E* **95**, 012147 (2017).
- [47] L. van Hove, *Physica* **16**, 137 (1950).
- [48] J. Cuesta and A. Sanchez, *J. Stat. Phys.* **115**, 869 (2004), FisEs 2002 Meeting, Tarragona, SPAIN, 2002.
- [49] D. A. Kofke and A. J. Post, *J. Chem. Phys.* **98**, 4853 (1993).
- [50] I. E. Kamenetskiy, K. K. Mon, and J. K. Percus, *J. Chem. Phys.* **121**, 7355 (2004).
- [51] S. Varga, G. Balló, and P. Gurin, *J. Stat. Mech.: Theory Exp.* **2011**, P11006 (2011).

- [52] P. Gurin and S. Varga, *J. Chem. Phys.* **139**, 244708 (2013).
- [53] M. J. Godfrey and M. A. Moore, *Phys. Rev. E* **89**, 032111 (2014).
- [54] J. L. Lebowitz, J. K. Percus, and J. Talbot, *J. Stat. Phys.* **49**, 1221 (1987).
- [55] P. Gurin and S. Varga, *Phys. Rev. E* **82**, 041713 (2010).
- [56] P. Gurin and S. Varga, *Phys. Rev. E* **83**, 061710 (2011).
- [57] P. Gurin and S. Varga, *J. Chem. Phys.* **142**, 224503 (2015).
- [58] J. F. Robinson, M. J. Godfrey, and M. A. Moore, *Phys. Rev. E* **93**, 032101 (2016).
- [59] M. González-Pinto, Y. Martínez-Ratón, S. Varga, P. Gurin, and E. Velasco, *J. Phys.: Condens. Matter* **28**, 244002 (2016).
- [60] J. Percus and M. Zhang, *Mol. Phys.* **69**, 347 (1990).
- [61] Y. Martínez-Ratón and E. Velasco, *Phys. Rev. E* **87**, 052314 (2013).
- [62] C. E. Sitta, F. Smallenburg, R. Wittkowski, and H. Löwen, *Phys. Chem. Chem. Phys.* **20**, 5285 (2018).
- [63] P. Gurin, G. Odriozola, and S. Varga, *Phys. Rev. E* **95**, 042610 (2017).
- [64] Z. W. Salsburg, R. W. Zwanzig, and J. G. Kirkwood, *J. Chem. Phys.* **21**, 1098 (1953).
- [65] L. Tonks, *Phys. Rev.* **50**, 955 (1936).
- [66] T. Iwaki, C.-Y. Shew, and G. Gumbs, *J. Chem. Phys.* **123**, 124712 (2005).
- [67] Y. Hu, L. Fu, and P. Charbonneau, *ArXiv e-prints* (2018), arXiv:1804.00693 [cond-mat.soft].
- [68] E. Velasco and P. Tarazona, *Phys. Rev. A* **42**, 7340 (1990).
- [69] A. G. Schlijper and R. Kikuchi, *J. Stat. Phys.* **61**, 143 (1990).
- [70] A. G. Schlijper and C. K. Harris, *J. Chem. Phys.* **95**, 7603 (1991).
- [71] D. de las Heras and M. Schmidt, *Phys. Rev. Lett.* **113**, 238304 (2014).